ACS OMEGA

http://pubs.acs.org/journal/acsodf

Article

New Insights into Phase Separation of Cerium Hydrides under Pressure

Xiaoqiu Ye,* Huan Li, and Shichang Li

Cite This: *ACS Omega* 2022, 7, 15681−15687

Read Online

ACCESS | Metrics & More | Article Recommendations | Supporting Information

ABSTRACT: We report theoretical calculations of the static ground-state structures and pressure-induced phase transformations of four cerium hydrides: CeH, CeH_2, $CeH_{2.5}$, and CeH_3. Under pressure, the experimental CaF_2-type structure of CeH_2 is likely to disproportionate to face-centered cubic (fcc) Ce and a cubic $Pm\bar{3}n$ (β-UH_3 type) structure of CeH_3 above 6 GPa. At further increasing pressures, fcc Ce will transform to a tetragonal $I4/mmm$ structure above 12 GPa, while CeH_3 moves through the following sequence of phases: $Pm\bar{3}n$ (β-UH_3 type) → $Pm\bar{3}n$ (A15 type) → $R\bar{3}m$; the corresponding transition pressures are calculated to be 10 and 70 GPa, respectively. The tetragonal $I4_1/amd$ structure of $CeH_{2.5}$ has the similar decomposition as that of CeH_2. Finding this previously unreported pressure-induced decomposition of CeH_2 will pave the way for investigations on the nature of hydrogen−metal interactions.

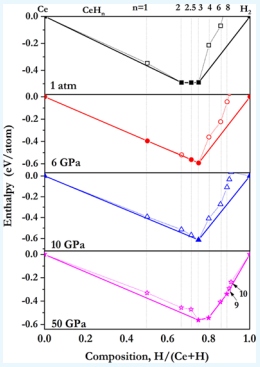

1. INTRODUCTION

Rare-earth metal hydrides are suitable compounds to study the hydrogen−metal interactions[1,2] since they have various electronic and structural transitions depending on hydrogen concentration, such as metal−insulator transition (MIT), lattice contraction from dihydrides to trihydrides of rare-earth metals,[3] and pressure-induced disproportionation of dihydrides.[4]

The formation of NaCl-type monohydride is likely a common behavior for the disproportionation of rare-earth metal dihydrides, as observed for LaH_2, YH_2, and ScH_2.[4] We also found that NaCl-type monohydride of plutonium can also be formed by PuH_2 above 62 GPa on the basis of first-principles density functional theory.[5] However, up to now, there is no direct study on the pressure-induced disproportionation of CeH_2. In fact, even the stable phases of CeH_2 and CeH_3 under pressure are still not very clear. Theoretically, Priyanga et al.[6] predicted a structural phase transition from fcc ($Fm\bar{3}m$, CaF_2 type) to hexagonal close-packed(hcp) ($P6/mmm$, AlB_2 type) of CeH_2 at 52 GPa, while for CeH_3, the phase transition pressure is about 4 GPa from fcc ($Fm\bar{3}m$, BiF_3 type) to hcp ($P6_3/mmc$, LaF_3 type). Peng et al.[7] also think that there is a phase transition from $Fm\bar{3}m$ to $P6/mmm$ for CeH_2, but the transition pressure was predicted to be 33 GPa; CeH_3 will transform to the $R\bar{3}m$ phase from the fcc phase at around 50 GPa. Recently, Salke et al.[8] found that pressurization of CeH_2 in the presence of H_2 up to 33 GPa did not result in any changes in the crystal structure. However, microsecond pulsed laser heating of ∼2000 K carried out at 33 GPa resulted in the formation of β-UH_3-type $Pm\bar{3}n$ CeH_3, which proved to be stable with further compression up to 80 GPa. Xin Li et al.[9] think that further hydrogenation of CeH_2 to form CeH_3 can easily occur when H_2 is excessive in the diamond anvil cell (DAC) chamber since CeH_3 has a lower calculated enthalpy value than that of CeH_2. Above 33 GPa, the distorted fcc phase of CeH_3 gradually transfers to another new cubic phase ($Pm\bar{3}n$, A15 type), and A15 $Pm\bar{3}n$ CeH_3 is stable up to 72 GPa in the presence of H_2. Li et al.[10] predicted that CeH_2 can be stable until 39 GPa; for CeH_3, the A15-type $Pm\bar{3}n$ phase transformed into the $R\bar{3}c$ phase at 53 GPa.

With this under consideration, the present work was devoted to check whether there is a pressure-induced disproportionation of CeH_2 by conducting a theoretical exploration of phase transformations of four cerium hydrides under pressure: CeH, CeH_2, $CeH_{2.5}$, and CeH_3. The results may shed light on the fundamental principles for understanding the nature of hydrogen−metal interactions.

2. RESULTS AND DISCUSSION

2.1. Stabilities for Different Stoichiometries under Pressure. To predict stable phases in the Ce-H system, the enthalpies of candidate structures of CeH_n (n = 1, 2, 2.5, 3) found by us are plotted in a typical convex hull diagram, indicating compositions relative to Ce + solid H_2 at selected pressures, in Figure 1; this can be also seen in Figure S1 in the

Received: January 24, 2022
Accepted: March 22, 2022
Published: April 30, 2022

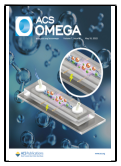

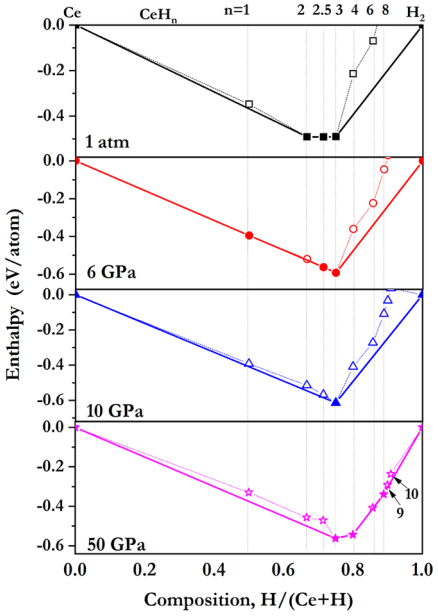

Figure 1. Convex hulls of the Ce-H system at selected pressures with ZPE included. The stoichiometric index n (in CeH_n) is indicated at the top. The compositions on the solid lines are stable at the corresponding pressure, while those on the dashed lines are unstable with respect to decomposition or disproportionation into other hydrides and potentially molecular hydrogen. The reference phases of solid hydrogen are from Labet's work.[11]

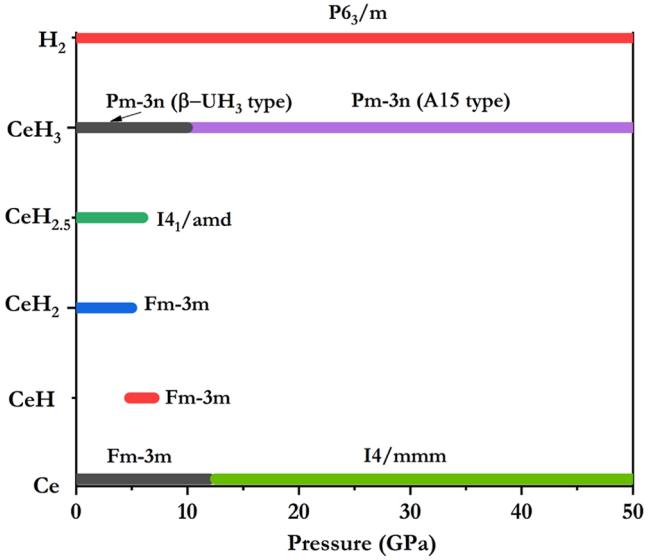

Figure 2. Pressure–composition phase diagram of theoretically predicted stable phases in the Ce-H system from 1 atm to 50 GPa with inclusion of ZPEs.

Supporting Information. We plotted previously predicted Ce polyhydrides[8] in the diagram: CeH_4-$I4/mmm$, CeH_6-$P6_3mc$, CeH_8-$P6_3mc$, CeH_9-$P6_3/mmc$, and CeH_{10}-$Fm\bar{3}m$. It is important to consider the zero-point energies (ZPEs) when determining the energetics of systems containing light atoms, and the enthalpies plotted in Figure 1 also include ZPEs. The detailed enthalpy curves of CeH_n (n = 1, 2, 2.5, 3) are listed in Figures S2–S5 in the Supporting Information.

As can be seen in Figure 1, CeH, CeH_2, $CeH_{2.5}$, and CeH_3 are very stable with respect to decomposition into the elements. Indeed, CeH_2, $CeH_{2.5}$, and CeH_3 are known experimentally, and as expected, they are all stable at 1 atm. CeH_2 is the global thermodynamic minimum at 1 atm, while CeH_3 achieves a global thermodynamic minimum above 6 GPa. This is consistent with the experimental observation.[12] Similar to the monohydride of La,Y, and Sc being stable at high pressures,[4] CeH is stable but in a very narrow pressure range near 6 GPa.

Interestingly, CeH, CeH_2, and $CeH_{2.5}$ will decompose into Ce and CeH_3 above 6 GPa through disproportionation reactions. Pure Ce can be obtained by squeezing cerium hydrides, which has not been reported before to the best of our knowledge. On the other hand, it also indicates that CeH_2 will decompose before undergoing any crystal structural changes above 10 GPa, not like the previous suggestions that CeH_2 is stable up to 33 GPa.[6−8] Figure 2 shows, in another way, the range of stabilities of different stoichiometries of cerium hydrides. All the thermodynamically stable phases are also dynamically stable (see Figures S9–S12). Interestingly, we found that $Fm\bar{3}m$ CeH_2 is not dynamically stable above 20 GPa (see Figure S10a), which also indicates that CeH_2 may undergo pressure-induced phase transitions or disproportionation reactions.

We will return to the interconversions between the various structures after presenting initial discussion of the calculated structural types.

2.2. Predicted CeHn (n = 1,2,2.5,3) Structures. CeH_2, $CeH_{2.5}$, and CeH_3 are the experimentally known cerium hydrides. The structure search readily reproduced the observed structure of CeH_2 and $CeH_{2.5}$ at 1 atm. At 1 atm, CeH_2 adopts the CaF_2-type crystal structure ($Fm\bar{3}m$, Z = 4, Figure 3a). All hydrogens occupy the tetrahedral holes of the fcc lattice. The calculated Ce-H separations of 2.35 Å match the experimental crystallographic values at P = 1 atm.[12] $CeH_{2.5}$ adopts the tetragonal $I4_1/amd$ structure (Z = 8, Figure 3b). This structure is similar to an alternative combination of fcc CeH_2 and fcc CeH_3. Hydrogens occupy the tetrahedral (T) and octahedral (O) holes of the lattice with Ce-H separations between 2.32 and 2.71 Å at 1 atm. This is in accordance with the trend that extra H atoms enter into the octahedral interstices during the formation of continuous solid solution CeH_x ($2.0 < x < 3.0$).[12]

Interestingly, at 1 atm, we find several new structures that are calculated to be more stable enthalpically than the suggested $Fm\bar{3}m$ CeH_3 (Z = 4, Figure 3c), and $Fm\bar{3}m$ CeH_3 is also dynamically unstable under atmospheric pressure (see Figure S12a). The most stable phase we calculate is the cubic $Pm\bar{3}n$ (β-UH_3 type) structure (Z = 8, Figure 3d), in which hydrogen atoms are tetrahedrally coordinated by Ce, with Ce-H separations between 2.32 and 2.39 Å at 1 atm. β-UH_3-type CeH_3 was also found recently in the experiment of Salke.[8] However, compared with $Pm\bar{3}n$ CeH_3, $Fm\bar{3}m$ CeH_3 can be easily synthesized by the reaction of cerium and hydrogen at normal pressure. We doubt that there may be a kinetic barrier to the transition between $Pm\bar{3}n$ CeH_3 and $Fm\bar{3}m$ CeH_3. This requires further research. As we know, one of the attractive structural properties exists in the Ce-H system is the lattice contraction from CeH_2 to CeH_3.[3] The predicted structures of CeH_2, $CeH_{2.5}$, and CeH_3 reproduce this experimental observation well.

Above 10 GPa, the β-UH_3-type $Pm\bar{3}n$ structure transformed to the A15 type $Pm\bar{3}n$ structure (Z = 2, Figure 4a), in which hydrogen atoms are also tetrahedrally coordinated by Ce, with

https://doi.org/10.1021/acsomega.2c00487
ACS Omega 2022, 7, 15681−15687

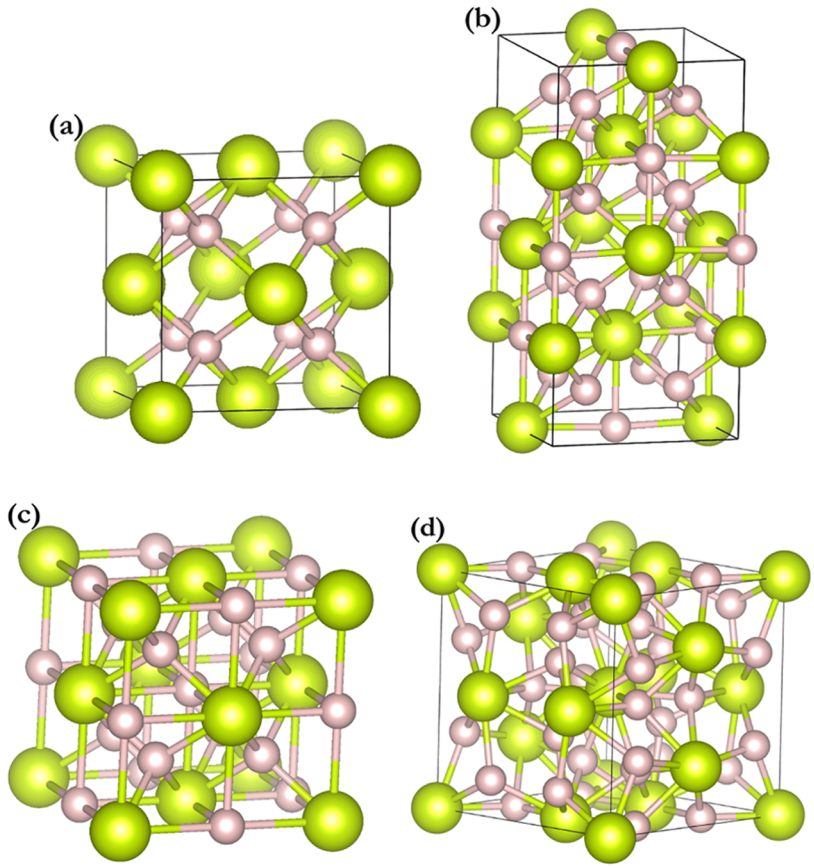

Figure 3. Predicted ground-state static structures of CeH_2, $CeH_{2.5}$, and CeH_3 at 1 atm. (a) $Fm\bar{3}m$ CeH_2, (b) $I4_1/amd$ $CeH_{2.5}$, (c) $Fm\bar{3}m$ CeH_3, and (d) $Pm\bar{3}n$ (β-UH_3 type) CeH_3. Large balls are Ce, and small balls are hydrogen. Lines are drawn for Ce-H separations shorter than 2.71 Å.

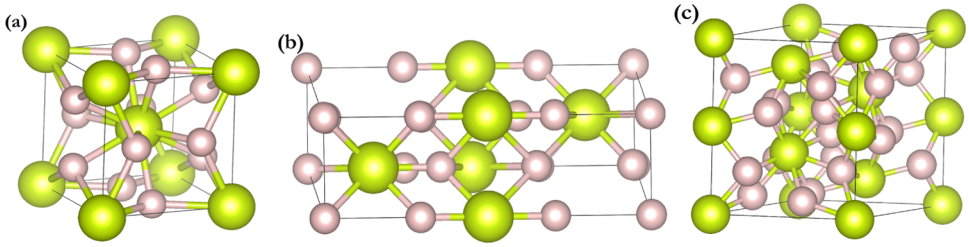

Figure 4. Predicted ground-state static structures of CeH_3. (a) A15 $Pm\bar{3}n$ CeH_3 at 50 GPa, (b) $R\bar{3}m$ CeH_3 at 100 GPa, and (c) $R\bar{3}c$ CeH_3 at 50 GPa. Large balls are Ce, and small balls are hydrogen. Lines are drawn for Ce-H separations shorter than 2.30 Å.

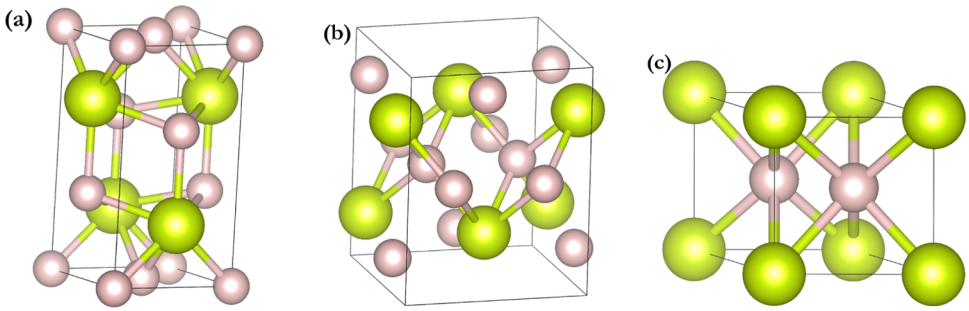

Figure 5. Predicted ground-state static structures of CeH_2. (a) $P4/nmm$ CeH_2 at 20 GPa, (b) $C2/m$ CeH_2 at 50 GPa, (c) $P6/mmm$ CeH_2 at 100 GPa. Large balls are Ce, and small balls are hydrogen. Lines are drawn for Ce-H separations shorter than 2.30 Å.

Ce-H separations of 2.13 Å at 50 GPa. The hexagonal $R\bar{3}m$ structure (Figure 4b) becomes thermodynamically stable relative to the A15-type $Pm\bar{3}n$ structure at 70 GPa, in which hydrogen atoms are tetrahedrally and octahedrally coordinated by Ce, with Ce-H separations between 2.03 and 2.27 Å at 100 GPa. The evolution of H coordination in CeH_3 with increasing pressure, from tetrahedral to octahedral, is consistent with the anticipated generalization that the number of neighbors of a

https://doi.org/10.1021/acsomega.2c00487
ACS Omega 2022, 7, 15681−15687

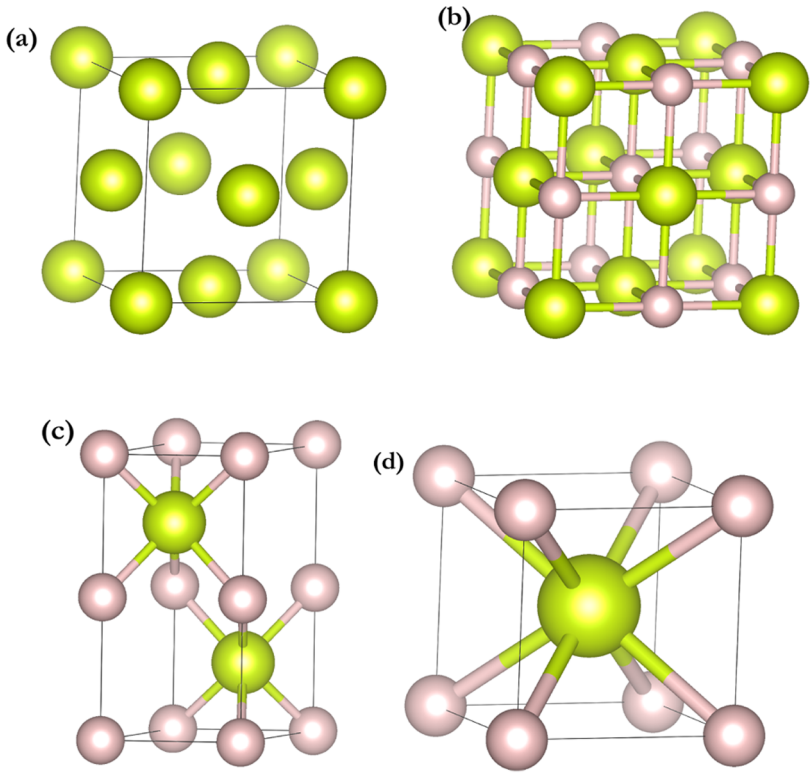

Figure 6. Predicted ground-state static structures of Ce and CeH. (a) $Fm\bar{3}m$ Ce at 0 GPa, (b) $Fm\bar{3}m$ CeH at 0 GPa, (c) $P6_3/mmc$ CeH at 20 GPa, and (d) $Pm\bar{3}m$ CeH at 50 GPa. Large balls are Ce, and small balls are hydrogen. Lines are drawn for Ce-H separations shorter than 2.51 Å.

hydrogen-occupied site is likely to increase with increasing pressure. Note that especially, the hexagonal $R\bar{3}c$ (Z = 6, Figure 4c) structure reported by Li et al[10] is the metastable phase, and depending on the tolerance used in the automated symmetry assignment (CASTEP with tolerance larger than 0.01), the program assigns the $R\bar{3}c$ structure to the A15-type $Pm\bar{3}n$ symmetry below 80 GPa.

The ground-state static phase transition sequence of CeH_2 during the pressure increase to 100 GPa is $Fm\bar{3}m$ → $P4/nmm$ (tetragonal, Z = 2, Figure 5a) → $C2/m$ (monoclinic, Z = 4, Figure 5b) → $P6/mmm$ (MgB_2-type, Z = 1, Figure 5c); the corresponding transition pressures are 10, 24, and 95 GPa with ZPEs included, respectively (see Figure S3). These similar high pressure phases of CeH_2 also emerged in ScH_2.[13]

As expected, we reproduced the previously suggested rock-salt structure for CeH at 1 atm (Z = 4, Figure 6b) with hydrogen atoms octahedrally coordinated by Ce. At 15 GPa, a new static structure emerges. This is a hexagonal $P6_3/mmc$ structure (Z = 2, Figure 6c), in which hydrogen atoms are also octahedrally coordinated by Ce, with Ce-H separations of 2.32 Å at 20 GPa. Above ∼50 GPa, the cubic $Pm\bar{3}m$ structure (Z = 1, Figure 6d) becomes thermodynamically stable relative to the $P6_3/mmc$ structure, in which hydrogen atoms are body-centered by Ce, with Ce-H separations of 2.33 Å at 50 GPa.

2.3. Disproportionations. With the phase transition sequences of CeH, CeH_2, $CeH_{2.5}$, and CeH_3 in hand (see Figures S2−S5), we can approach the pressure dependence of the CeH_2 disproportionation reaction. Figure 7 compares the enthalpies of the reactions

$$CeH_2 \rightarrow 1/2CeH + 1/2\ CeH_3$$

$$CeH_2 \rightarrow 1/3Ce + 2/3\ CeH_3$$

with and without ZPEs. Positive enthalpies mark a region of stability of CeH_2, and negative ones mark that of CeH + CeH_3 or Ce + CeH_3.

Figure 7 shows that CeH_2 is enthalpically stable below 5 GPa but becomes unstable compared to Ce, CeH, and CeH_3 at higher pressure. Pure Ce can be formed by the pressure-induced disproportionation of CeH_2 above 6 GPa. This is different from the case of MH_2 (M = Sc, Y, and La),[4] in which MH_2 decomposed to MH and MH_3 under high pressure; no pure metal was found. Note that especially, Salke et al.[8] found that pressurization of CeH_2 in a H_2 atmosphere up to 33 GPa did not result in any changes in the crystal structure. This is not in accordance with our results and the phenomenon of disproportionation reactions of MH_2 (M = Sc, Y, and La).[4] In the case of excessive H_2, CeH_2 can easily react with H_2 to form CeH_3, which was also confirmed by the experiment of Li.[9] Salke[8] found that the mixture of CeH_2 and H_2 up to 33 GPa did not result in any changes in X-ray diffraction (XRD) spectra, which may be due to the difficulty in distinguishing the XRD peaks between CeH_2 and CeH_3. In this work, CeH_2 was pressurized alone in the absence of H_2, and it is found that when the pressure reaches a certain value, CeH_2 will decompose to form Ce and CeH_3.

Interestingly, $CeH_{2.5}$ also has a similar disproportionation trend as that of CeH_2 (see Figure S7). Our results confirmed that the disproportionation reactions of MH_{2+x} (M = rare-earth metals, $0 \leq x < 1$) under high pressure are likely common behaviors. However, for CeH_{2+x} ($0 \leq x < 1$), pure Ce can be formed under high pressure due to the disproportionation reaction. Indeed, CeH is stable but in a very narrow pressure range near 6 GPa (see Figures 2 and S6), which is to say that CeH_2 or $CeH_{2.5}$ is likely to disproportionate to CeH and

https://doi.org/10.1021/acsomega.2c00487
ACS Omega 2022, 7, 15681−15687

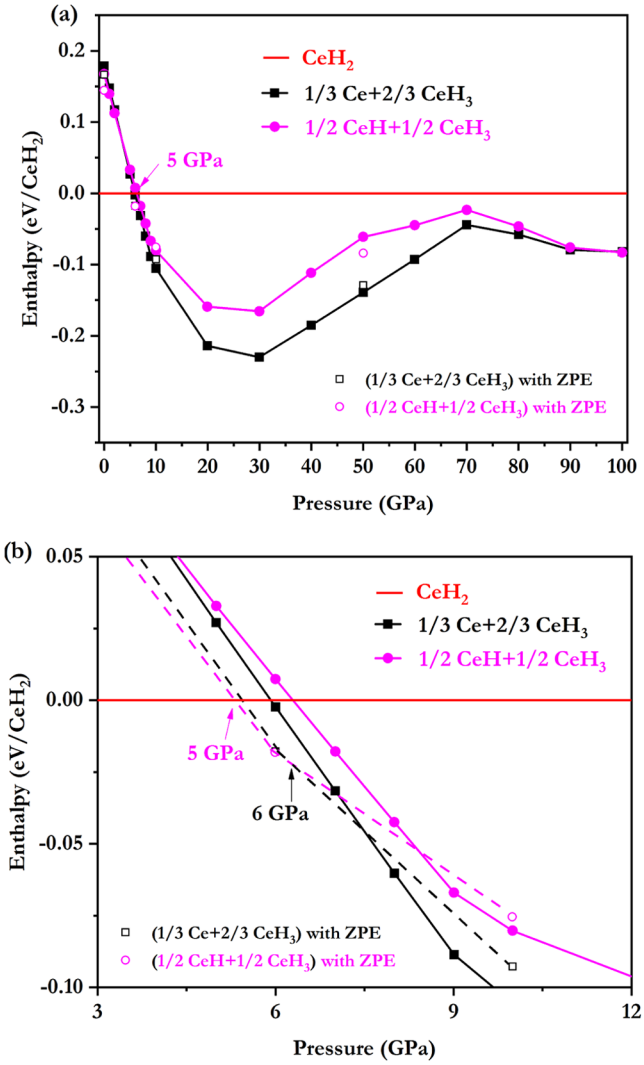

Figure 7. Static ground-state enthalpy curves per formula unit (magenta and black curves) as a function of pressure with respect to CeH_2. We also move beyond the static approximation by estimating the contribution of ZPEs (dashed lines). We have considered the most stable structures for Ce, CeH, CeH_2, and CeH_3 found in this work at the specified pressure ranges. The ZPE differences are taken to be approximately pressure-independent. (a) Enthalpy curves between 0 and 100 GPa. (b) Enthalpy curves between 3 and 12 GPa.

CeH_3, and then, CeH continues to disproportionate to Ce and CeH_3, as shown in Figure S6.

To elucidate the mechanisms for the pressure-induced disproportionation of CeH_2 leading to the formation of Ce and CeH_3, we examined the evolution of the internal energy (U) and the product of pressure and volume (PV), which contribute to the enthalpy ($H = U + PV$) of the pertinent material systems and phases in response to pressure change. We show in Figure 8 the pressure dependence of ΔU, $\Delta(PV)$, and ΔH, defined as the values for the mixture of 1/3 Ce + 2/3 CeH_3 relative to that for CeH_2, which are set to zero. It is seen clearly that the transition from CeH_2 to the 1/3 Ce + 2/3 CeH_3 mixture is caused by the decrease in the internal energy of the latter; meanwhile, the PV term rises with increasing pressure, although its large negative magnitude is still the main contributor to the overall negative relative enthalpy around the phase transition pressure. Between 10 and 30 GPa, both the U and PV terms make similar contributions to lowering the

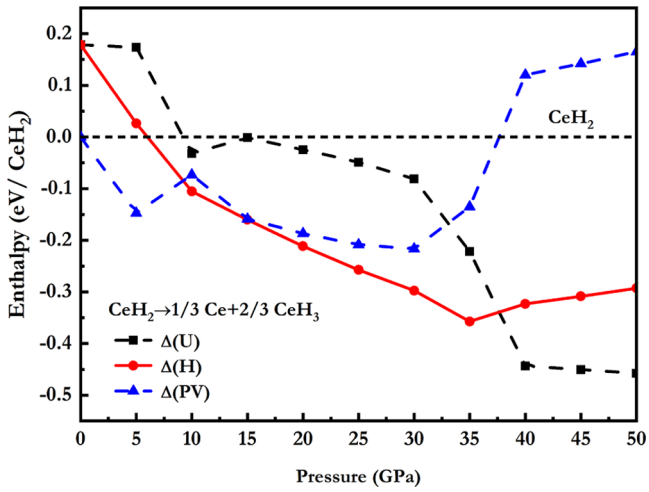

Figure 8. Calculated ΔH, ΔU, and $\Delta(PV)$ versus pressure for the predicted phase transitions: $CeH_2 \rightarrow$ 1/3 Ce + 2/3 CeH_3, where CeH_2 is chosen as the reference phase. We have considered the most stable structures for Ce, CeH_2, and CeH_3 found in this work at the specified pressure ranges.

enthalpy. After 35 GPa, the large negative magnitude of U overcompensates for the increasing PV term, resulting in the stabilization of the 1/3 Ce + 2/3 CeH_3 mixture relative to CeH_2.

For Ce−Ce separations, the number of nearest neighbors in Ce ($I4/mmm$, $Z = 2$) is larger than that of CeH_2 ($C2/m$, $Z = 4$) at 50 GPa, as shown in Figure S13a, while for Ce-H, the number of nearest neighbors in CeH_3 (A15 type $Pm\bar{3}n$, $Z = 2$) is larger than that of CeH_2 ($C2/m$, $Z = 4$) at 50 GPa (see Figure S13b). It indicates that compared with CeH_2, the Ce−Ce bonding in the $I4/mmm$ phase of Ce and the Ce−H bonding in the $Pm\bar{3}n$ phase of CeH_3 may increase as well. We then calculated the projected crystal orbital Hamilton population (pCOHP)[14] between Ce−Ce, Ce−H, and H−H pairs in Ce, CeH_2, and CeH_3 all at 50 GPa, as shown in Figure S14. Compared with CeH_2, the Ce−Ce bonding in the $I4/mmm$ phase of Ce and the Ce−H bonding in the $Pm\bar{3}n$ phase (A15 type) of CeH_3 are strengthened. It suggests that the increasing Ce−Ce bonding in the $I4/mmm$ phase of Ce and the increasing Ce−H bonding in the $Pm\bar{3}n$ phase of CeH_3 may play an important role in the phase transition and stabilization. The calculated electronic structures show that each phase of CeH_n (n = 1, 2, 2.5, 3) is metallic. Hydrogen in CeH_n (n = 1, 2, 2.5, 3) has the form of $H^{\delta-}$ (δ = 0.55−0.72), as can be seen in Table S1. Histograms (Figure S13) also show that the nearest distance of H−H in CeH_n (n = 1, 2, 2.5, 3) is around 2 Å. Thus, no cage-like structure of hydrogen is formed as repored in cerium polyhydrides.

3. CONCLUSIONS

In summary, we have explored pressure-induced phase transformations of four cerium hydrides: CeH, CeH_2, $CeH_{2.5}$, and CeH_3. We find an unusual circumstance; CeH, CeH_2, and $CeH_{2.5}$ will decompose into Ce and CeH_3 above 6 GPa through disproportionation reactions. Pure Ce can be obtained by squeezing cerium hydrides, which is different from the case of MH_2 (M = Sc,Y, and La), in which MH_2 decomposed to MH and MH_3 under high pressure; no pure metal was found. Indeed, CeH_2 or $CeH_{2.5}$ is also likely to disproportionate to CeH and CeH_3, and then, CeH continues to disproportionate

https://doi.org/10.1021/acsomega.2c00487
ACS Omega 2022, 7, 15681−15687

to Ce and CeH_3 since CeH is only stable in a very narrow pressure range near 6 GPa. The increasing Ce−Ce bonding in pure Ce and the increasing Ce−H bonding in CeH_3 may play an important role in the disproportionation reactions of CeH, CeH_2, and $CeH_{2.5}$. The theoretical work indicates that pure metal and its higher hyrides may also be obtained in other metal−hydrogen system.

4. METHODS AND COMPUTATIONAL DETAILS

We searched extensively for CeH_n (n = 1, 2, 2.5, 3) ground-state structures at 0 K using the particle swarm optimization methodology implemented in the CALYPSO code.[15] This method has been applied successfully to a wide range of crystalline systems ranging from elemental solids to binary and ternary compounds.[15] Our structure searches with system sizes containing up to 6 formula units (fu) per simulation cell were performed at pressures of 0−100 GPa. Each generation contains 30 structures. We usually follow 50 generations to achieve a converged structure.

The underlying structural relaxations were carried out at 0 K using density functional theory using the Perdew−Burke−Ernzerhof (PBE) exchange−correlation functional[16] as implemented in the VASP code.[17] The projector-augmented wave method[18] was adopted, with $1s^1$ (cutoff radius of $1.1a_0$) and $5s^25p^64f^15d^16s^2$ (cutoff radius of $2.7a_0$) treated as valence electrons for H and Ce, respectively. An energy cutoff of 800 eV and dense Monkhorst−Pack[19] k-meshes with a grid spacing of $2\pi \times 0.03$ Å^{-1} gave good convergence of the structural relaxations (see Figure S16). Phonon calculations were carried out using VASP in conjunction with the PHONOPY code.[20] Given the light hydrogens in the structure, vibrational contributions to the relative enthalpy were considered.

ASSOCIATED CONTENT

Supporting Information

The Supporting Information is available free of charge at https://pubs.acs.org/doi/10.1021/acsomega.2c00487.

> Theoretical cerium−hydrogen phase diagram, enthalpy curves, phonon densities of states, electronic properties, structural parameters, and supporting calculation details (PDF)

AUTHOR INFORMATION

Corresponding Author

Xiaoqiu Ye − *Science and Technology on Surface Physics and Chemistry Laboratory, Mianyang 621908, China;* orcid.org/0000-0003-4075-8556; Email: xiaoqiugood@sina.com

Authors

Huan Li − *Science and Technology on Surface Physics and Chemistry Laboratory, Mianyang 621908, China*

Shichang Li − *School of Science, Chongqing University of Posts and Telecommunications, Chongqing 400065, China*

Complete contact information is available at: https://pubs.acs.org/10.1021/acsomega.2c00487

Notes

The authors declare no competing financial interest.

ACKNOWLEDGMENTS

The authors are grateful to Roald Hoffmann from Cornell University, Martin Rahm from Chalmers University of Technology, Hui Wang from Jilin University, and Li Huang, Ce Ma, Xiao Tan, Liuhua Xie, and Ruizhi Qiu from Science and Technology on Surface Physics and Chemistry Laboratory for their discussions. We acknowledge the support by the National Natural Science Foundation of China (Grants Nos. 21401173, 21371160, and 11305147).

REFERENCES

(1) Sun, W.; Kuang, X.; Keen, H. D. J.; Lu, C.; Hermann, A. Second group of high-pressure high-temperature lanthanide polyhydride superconductors. *Phys. Rev. B* **2020**, *102*, No. 144524.

(2) Chen, W.; Semenok, D. V.; Huang, X.; Shu, H.; Li, X.; Duan, D.; Cui, T.; Oganov, A. R. High-Temperature Superconducting Phases in Cerium Superhydride with a T_c up to 115 K below a Pressure of 1 Megabar. *Phys. Rev. Lett.* **2021**, *127*, No. 117001.

(3) Ao, B. Y.; Wang, X. L.; Shi, P.; Chen, P. H.; Ye, X. Q.; Lai, X. C.; Ai, J. J.; Gao, T. Lattice contraction of cerium hydrides from first-principles LDA + U calculations. *Int. J. Hydrog. Energy* **2012**, *37*, 5108−5113.

(4) Machida, A.; Honda, M.; Hattori, T.; Sano-Furukawa, A.; Watanuki, T.; Katayama, Y.; Aoki, K.; Komatsu, K.; Arima, H.; Ohshita, H.; et al. Formation of NaCl-Type Monodeuteride LaD by the Disproportionation Reaction of LaD_2. *Phys. Rev. Lett.* **2012**, *108*, No. 205501.

(5) Li, S. C.; Ao, B. Y.; Ye, X. Q.; Qiu, R. Z.; Gao, T. New insights into the crystal structures of plutonium hydrides from first-principles calculations. *J. Phys. Chem. C* **2018**, *122*, 10103−101121.

(6) Priyanga, G. S.; Rajeswarapalanichamy, R.; Iyakutti, K. First principles study of structural, electronic, elastic and magnetic properties of cerium and praseodymium hydrogen system REHx (RE: Ce, Pr and x = 2, 3). *J. Rare Earths* **2015**, *33*, 289−303.

(7) Peng, F.; Sun, Y.; Pickard, C. J.; Needs, R. J.; Wu, Q.; Ma, Y. M. Hydrogen Clathrate Structures in Rare Earth Hydrides at High Pressures: Possible Route to Room-Temperature Superconductivity. *Phys. Rev. Lett.* **2017**, *119*, No. 107001.

(8) Salke, N. P.; Davari Esfahani, M. M.; Zhang, Y.; Kruglov, I. A.; Zhou, J.; Wang, Y.; Greenberg, E.; Prakapenka, V. B.; Liu, J.; Oganov, A. R.; Lin, J. F. Synthesis of clathrate cerium superhydride CeH_9 at 80-100 GPa with atomic hydrogen sublattice. *Nat. Commun.* **2019**, *10*, No. 4453.

(9) Li, X.; Huang, X.; Duan, D.; Pickard, C. J.; Cui, T.; et al. Polyhydride CeH_9 with an atomic-like hydrogen clathrate structure. *Nat. Commun.* **2019**, *10*, No. 3461.

(10) Li, B.; Miao, Z. L.; Ti, L.; Liu, S. L.; Chen, J.; Shi, Z. X.; Gregoryanz, E. Predicted high-temperature superconductivity in cerium hydrides at high pressures. *J. Appl. Phys.* **2019**, *126*, No. 235901.

(11) Labet, V.; Hoffmann, R.; Ashcroft, N. W. A fresh look at dense hydrogen under pressure. III. Two competing effects and the resulting intra-molecular H-H separation in solid hydrogen under pressure. *J. Chem. Phys.* **2012**, *136*, No. 074503.

(12) Manchester, F. D.; Pitre, J. M. The Ce-H (cerium-hydrogen) system. *J. Phase Equilib.* **1997**, *18*, No. 63.

(13) Ye, X. Q.; Hoffmann, R.; Ashcroft, N. W. Theoretical Study of Phase Separation of Scandium Hydrides under High Pressure. *J. Phys. Chem. C* **2015**, *119*, 5614−5625.

(14) Maintz, S.; Deringer, V. L.; Tchougréeff, A. L.; Dronskowski, R. LOBSTER: A tool to extract chemical bonding from plane-wave based DFT. *J. Comput. Chem.* **2016**, *37*, 1030−1035.

(15) Wang, Y.; Lv, J.; Zhu, L.; Ma, Y. Crystal structure prediction via particle-swarm optimization. *Phys. Rev. B* **2010**, *82*, No. 094116.

(16) Perdew, J. P.; Burke, K.; Ernzerhof, M. Generalized Gradient Approximation Made Simple. *Phys. Rev. Lett.* **1996**, *77*, 3865−3868.

(17) Kresse, G.; Furthmüller, J. Efficient iterative schemes for ab initio total-energy calculations using a plane-wave basis set. *Phys. Rev. B* **1996**, *54*, 11169−11186.
(18) Blöchl, P. E. Projector augmented-wave method. *Phys. Rev. B* **1994**, *50*, 17953−17979.
(19) Monkhorst, H. J.; Pack, J. D. Special points for Brillouin-zone integrations. *Phys. Rev. B* **1976**, *13*, 5188−5192.
(20) Togo, A.; Oba, F.; Tanaka, I. First-principles calculations of the ferroelastic transition between rutile-type and $CaCl_2$-type SiO_2 at high pressures. *Phys. Rev. B* **2008**, *78*, No. 134106.

https://doi.org/10.1021/acsomega.2c00487
ACS Omega 2022, 7, 15681−15687